Absorption Enhancement in Solution Processed Metal-Semiconductor Nanocomposites

F. Pelayo García de Arquer,[1] Fiona J. Beck,[1] and Gerasimos Konstantatos[1,*]

[1]*ICFO – Institut de Ciènces Fotòniques, Mediterranean Technology Park, 08860 Castelldefels (Barcelona), Spain*
**gerasimos.konstantatos@icfo.es*

Abstract: We present a full wave 3D simulation study of optical absorption enhancement in solution processed metal-semiconductor nanocomposite ultrathin films, which consist of colloidal metallic nanoparticles (MNPs) and semiconductor matrices of polymer and colloidal quantum dots (CQD). We present an approach for modeling the optical properties of a CQD film, and study the effect of the optical properties of the semiconductor in the near field enhancement showing that CQD is a very promising platform to exploit the benefits of the near-field effects. We show that over a 100% enhancement can be achieved in the visible-near infrared region of the spectrum for CQD PbS films, with a maximum gain factor of 4 when MNPs are on resonance. We study in detail the effect of MNP capping for different ligand lengths and materials and propose solutions to optimize absorption enhancement.

OCIS codes: (040.5160) Photodetectors; (250.5403) Plasmonics; (310.6860).Thin films, optical properties.

References and links

1. G. Konstantatos and E. H. Sargent, "Nanostructured materials for photon detection," Nat. Nanotechnol. **5**(6), 391–400 (2010).
2. D. V. Talapin, J.-S. Lee, M. V. Kovalenko, and E. V. Shevchenko, "Prospects of colloidal nanocrystals for electronic and optoelectronic applications," Chem. Rev. **110**(1), 389–458 (2010).
3. J. M. Luther, J. Gao, M. T. Lloyd, O. E. Semonin, M. C. Beard, and A. J. Nozik, "Stability assessment on a 3% bilayer PbS/ZnO quantum dot heterojunction solar cell," Adv. Mater. (Deerfield Beach Fla.) **22**(33), 3704–3707 (2010).
4. J. P. Clifford, G. Konstantatos, K. W. Johnston, S. Hoogland, L. Levina, and E. H. Sargent, "Fast, sensitive and spectrally tuneable colloidal-quantum-dot photodetectors," Nat. Nanotechnol. **4**(1), 40–44 (2009).
5. J. M. Caruge, J. E. Halpert, V. Wood, V. Bulović, and M. G. Bawendi, "Colloidal quantum-dot light-emitting diodes with metal-oxide charge transport layers," Nat. Photonics **2**(4), 247–250 (2008).
6. I. Gur, N. A. Fromer, M. L. Geier, and A. P. Alivisatos, "Air-stable all-inorganic nanocrystal solar cells processed from solution," Science **310**(5747), 462–465 (2005).
7. A. G. Pattantyus-Abraham, I. J. Kramer, A. R. Barkhouse, X. Wang, G. Konstantatos, R. Debnath, L. Levina, I. Raabe, M. K. Nazeeruddin, M. Grätzel, and E. H. Sargent, "Depleted-heterojunction colloidal quantum dot solar cells," ACS Nano **4**(6), 3374–3380 (2010).
8. J. Tang and E. H. Sargent, "Infrared colloidal quantum dots for photovoltaics: fundamentals and recent progress," Adv. Mater. (Deerfield Beach Fla.) **23**(1), 12–29 (2011).
9. H. A. Atwater and A. Polman, "Plasmonics for improved photovoltaic devices," Nat. Mater. **9**(3), 205–213 (2010).
10. H. R. Stuart and D. G. Hall, "Enhanced Dipole-Dipole Interaction between Elementary Radiatiors Near a Surface," Phys. Rev. Lett. **80**(25), 5663–5666 (1998).
11. K. R. Catchpole and S. Pillai, "Surface plasmons for enhanced silicon light-emitting diodes and solar cells," J. Lumin. **121**(2), 315–318 (2006).
12. D. Derkacs, S. H. Lim, P. Matheu, W. Mar, and E. T. Yu, "Improved performance of amorphous silicon solar cells via scattering from surface Plasmon polaritons in nearby metallic nanoparticles," Appl. Phys. Lett. **89**(9), 093103 (2006).
13. Z. Ouyang, S. Pillai, F. Beck, O. Kunz, S. Varlamov, K. R. Catchpole, P. Campbell, and M. A. Green, "Effective light trapping in polycrystalline silicon thin-film solar cells by means of rear localized surface plasmons," Appl. Phys. Lett. **96**(26), 261109 (2010).

#151334 - $15.00 USD Received 18 Jul 2011; accepted 13 Sep 2011; published 7 Oct 2011

14. V. E. Ferry, M. A. Verschuuren, H. B. T. Li, E. Verhagen, R. J. Walters, R. E. I. Schropp, H. A. Atwater, and A. Polman, "Light trapping in ultrathin plasmonic solar cells," Opt. Express **18**(S2 Suppl 2), A237–A245 (2010).
15. K. R. Catchpole and A. Polman, "Plasmonic solar cells," Opt. Express **16**(26), 21793–21800 (2008).
16. F. J. Beck, E. Verhagen, S. Mokkapati, A. Polman, and K. R. Catchpole, "Resonant SPP modes supported by discrete metal nanoparticles on high-index substrates," Opt. Express **19**(S2 Suppl 2), A146–A156 (2011).
17. H. R. Stuart and D. G. Hall, "Thermodynamic limit to light trapping in thin planar structures," J. Opt. Soc. Am. A **14**(11), 3001–3007 (1997).
18. Z. Yu, A. Raman, and S. Fan, "Fundamental limit of nanophotonic light trapping in solar cells," Proc. Natl. Acad. Sci. U.S.A. **107**(41), 17491–17496 (2010).
19. H. Hiramatsu and F. E. Osterloh, "A Simple Large-Scale Synthesis of Nearly Monodisperse Gold and Silver Nanoparticles with Adjustable Sizes and with Exchangeable Surfactants," Chem. Mater. **16**(13), 2509–2511 (2004).
20. B. P. Rand, P. Peumans, and S. R. Forrest, "Long-range absorption enhancement in organic tandem thin-film solar cells containing silver nanoclusters," J. Appl. Phys. **96**(12), 7519–7527 (2004).
21. J. L. Wu, F.-C. Chen, Y.-S. Hsiao, F.-C. Chien, P. Chen, C.-H. Kuo, M. H. Huang, and C. S. Hsu, "Surface plasmonic effects of metallic nanoparticles on the performance of polymer bulk heterojunction solar cells," ACS Nano **5**(2), 959–967 (2011).
22. L.-J. Pegg, S. Schumann, and R. A. Hatton, "Enhancing the open-circuit voltage of molecular photovoltaics using oxidized Au nanocrystals," ACS Nano **4**(10), 5671–5678 (2010).
23. M. D. Brown, T. Suteewong, R. S. S. Kumar, V. D'Innocenzo, A. Petrozza, M. M. Lee, U. Wiesner, and H. J. Snaith, "Plasmonic dye-sensitized solar cells using core-shell metal-insulator nanoparticles," Nano Lett. **11**(2), 438–445 (2011).
24. J. B. Khurgin, G. Sun, and R. Soref, "Practical limits of absorption enhancement near metal nanoparticles," Appl. Phys. Lett. **94**(7), 071103 (2009).
25. J.-Y. Lee and P. Peumans, "The origin of enhanced optical absorption in solar cells with metal nanoparticles embedded in the active layer," Opt. Express **18**(10), 10078–10087 (2010).
26. Lumerical FDTD version 7 *http://www.lumerical.com*
27. V. Lucarini, *Kramers-Kronig Relations in Optical Materials Research*, Springer (2005).
28. M. Law, M. C. Beard, S. Choi, J. M. Luther, M. C. Hanna, and A. J. Nozik, "Determining the internal quantum efficiency of PbSe nanocrystal solar cells with the aid of an optical model," Nano Lett. **8**(11), 3904–3910 (2008).
29. I. Moreels, G. Allan, B. De Geyter, L. Wirtz, C. Delerue, and Z. Hens, "Dielectric function of colloidal lead chalcogenide quantum dos obtained by a Kramers-Krönig analysis of the absorbance spectrum," Phys. Rev. B **81**(23), 235319 (2010).
30. SOPRA N&K Database, *http://www.sopra-sa.com*
31. E. D. Palik, *Handbook of Optical Constants of Solids*, Academic Press, New York, (1998).
32. P. B. Johnson and R. W. Christy, "Optical constants of the noble metals," Phys. Rev. B **6**(12), 4370–4379 (1972).
33. C. F. Bohren and D. R. Huffman, *Absorption and Scattering of Light by Small Particles*, Wiley Interscience, New York, (1983).
34. Y. Kim, S. Cook, S. M. Tuladhar, S. A. Choulis, J. Nelson, J. R. Durrant, D. D. C. Bradley, M. Giles, I. McCulloch, C.-S. Ha, and M. Ree, "A strong regioregularity effect in self-organizing conjugated polymer films and high-efficiency polythiophene:fullerene solar cells," Nat. Mater. **5**(3), 197–203 (2006).
35. L. A. Sweatlock, S. A. Maier, H. A. Atwater, J. Penninkhof, and A. Polman, "Highly confined electromagnetic fields in arrays of strongly coupled Ag nanoparticles," Phys. Rev. B **71**(23), 235408 (2005).
36. A. Taleb, C. Petit, and M. Pileni, "Optical Properties of Self-Assembled 2D and 3D Superlattices of Silver Nanoparticles," J. Phys. Chem. B **102**(12), 2214–2220 (1998).
37. A. O. Pinchuk and G. C. Schatz, "Nanoparticle optical properties, Far- and near-field electrodynamic coupling in a chain of silver spherical nanoparticles," Mater. Sci. Eng. B **149**(3), 251–258 (2008).
38. V. R. Almeida, Q. Xu, C. A. Barrios, and M. Lipson, "Guiding and confining light in void nanostructure," Opt. Lett. **29**(11), 1209–1211 (2004).

1. Introduction

Solution-processed nanomaterials have opened new avenues towards low-cost, high performance optoelectronics [1]. Colloidal quantum dots (CQDs) combine the spectral tunability offered by the quantum confinement size effect [2], the robustness of inorganic materials [3] and the ease of processability from the solution phase. Progress in the field of CQD optoelectronics has led to the demonstration of efficient and low-cost photodetectors [1,4], light emitters [5] and solar cells [3,6,7].

Despite improvements in the electrical properties of colloidal quantum dot films, carrier mobilities in solar cell devices are measured on the order of 10^{-4}-10^{-3} cm^2/Vs [8]. For typical PbS quantum dot films at solar intensities, with carrier lifetimes of ≈10 μs and built-in electric fields of 0.3-0.5 eV, this entails a high-charge collection efficiency film thickness of 200-300

#151334 - $15.00 USD Received 18 Jul 2011; accepted 13 Sep 2011; published 7 Oct 2011

nm. The absorption of colloidal quantum dots, however, albeit on the order of 10^4 cm^{-1}, requires a total thickness of 500-700 nm for complete optical absorption. A gap, therefore, exists between electrically and optically active lengths in CQD device structures, limiting the EQEs of such devices to 30-50%. An approach that could effectively increase the absorption in quantum dot films at low cost, and without sacrifice in the electronic performance, would be an essential step towards high performance CQD detectors and solar cells.

The use of plasmonics to improve the performance of photodetectors and solar cells has experienced rapidly growing interest in the past decade (see for example [9] and references therein). Most of the efforts so far have been focused on light trapping via far-field scattering [10–14]. In this case, incident light is scattered by plasmonic nanostructures and coupled into trapped modes in the active region of the cell; either guided photonic modes or propagating modes that are totally internally reflected. Plasmonic nanostructures are of interest for this application due to the high scattering cross sections and coupling efficiencies that can be engineered [15,16]. However, to significantly increase the optical path length in thin cells light must undergo multiple scattering events. Absorption enhancement is thus very sensitive to the losses in the scattering structure. Even small amounts of Ohmic loss in the metal nanostructures and out-coupling of scattered light can result in significant reductions in light trapping efficiency. Additionally, for cells with ultra-thin active regions, such as quantum dot and polymer solar cells on the order of 100-300 nm thick, the number of guided photonic modes in the structure is restricted, reducing the overall broadband absorption enhancement that can be achieved [17,18].

In our current study, we thus turn our attention to small metal nanoparticles (MNPs), with diameters from 3 to 50 nm, which can be synthesized and processed in solution phase [19], offering processing compatibility with solution processed semiconductors. These MNPs can be readily blended with polymers and quantum dot solutions and yield metal-semiconductor nanocomposite thin films. In this size regime of MNPs, far-field scattering is not the major component of enhancement. The optical fields in this case are enhanced locally in the vicinity of the MNP, through the so-called "near field enhancement". In very thin cells supporting few photonic modes, absorption increase via near field enhancement may surpass that provided by far-field scattering structures.

These advantageous features of near-field absorption enhancement have attracted considerable interest in thin film solar cells, with some initially promising results in organic [20–22] and dye-sensitized solar cells [23]. The near field enhancement in such systems has been studied by the generalization of Mie scattering theory for absorbing media [24] and extension of these models to account for absorption enhancement in the host medium [25]. These models have proved very valuable in providing an understanding of the underlying physical mechanisms and some fundamental design guidelines for an MNP in an infinite host medium. However these models cannot easily consider specific device structures and account for multiple MNP interactions. We hereby employ a full-wave FDTD 3D simulation study [26] of MNP-Semiconductor nanocomposites, relevant to solar cell and photodetector device structures. This allows us to investigate the effect of MNP size and concentration, as well as the effects of the capping molecules (or ligands) of the MNPs on absorption enhancement, taking into account inter-particle interactions and substrate edge effects.

2. Optical modeling of CQDs

To model the absorption enhancement in CQDs PbS was chosen as a baseline material, because of its favorable properties for photodetectors and solar cells [8]. The optical properties of PbS CQD films (complex refractive index $n_{PbS,EM} + i\kappa_{PbS,EM}$) were determined from experimental absorbance by using the Kramers-Krönig (KK) relation [27]. Absorbance measurements were taken of PbS QDs in solution, with the exciton peak located at $\lambda = 945$ nm to get the spectral shape of a specific specimen. From this data the absorption coefficient, $\alpha(\lambda)$, is obtained by normalizing the absorption spectra such that $\alpha(\lambda = 945\ nm)$ at the exciton peak

#151334 - $15.00 USD Received 18 Jul 2011; accepted 13 Sep 2011; published 7 Oct 2011

is equal to literature values for similar material systems [4,28]. The extinction coefficient, $\kappa_{PbS,EM}(\lambda)$, is then calculated from $\alpha(\lambda)$. We then apply discrete form of the KK relation to determine $n_{PbS,EM}(\lambda)$ from $\kappa_{PbS,EM}(\lambda)$ and $\alpha(\lambda)$ [29]. Because absorption data is truncated to 0.4-2 μm, to avoid unphysical results derived from the discretization we normalize $n_{PbS,EM}(\lambda)$ to 2.2 at λ = 2 μm, where PbS is not absorbing and $\alpha(\lambda) = 0$. This value is obtained by calculating the effective refractive index at λ = 2μm for a hexagonal close-packed (HCP) PbS QD film consisting of 3 nm, butylamine capped QDs, where the $n_{PbS} = n_{PbS,bulk}$ [30] and n_{lig} = 1.5. We propose the obtained effective complex refractive index as a tool to qualitatively calculate absorption in PbS films, without having to model individual QDs in very complex geometries.

In order to validate that approach, we compared the calculated absorption of an HCP film to that of a homogenous layer with $n_{PbS,EM} + i\kappa_{PbS,EM}$ as calculated above, both with and without the presence of Ag MNPs. In Fig. 1(a) the QDs are modeled individually with $n = n_{bulk}\,\eta_{lig}$ and $\kappa = \kappa_{eff}/\eta_{lpacking}$ ($\eta_{lig} = V_{QD}/(V_{QD} + V_{lig})$ and $\eta_{lpacking} = 0.7$). The QDs are organized in a monolayer with HCP packing, embedded in an organic layer (n = 1.55) of 3 nm thickness to include ligand effects in the field distribution. In Fig. 1(b) the host is a uniform effective medium. In both cases the MNPs are distributed uniformly with a 2D lattice constant given by $d = D$xC. as above A plane wave x-polarized illuminates the sample from the top. Given this symmetry, periodic boundary conditions were applied to a unit cell in x and y directions, and perfectly matched layers were imposed to the z-axis. The refractive indices of the metals were modeled with the multi-coefficient fits of the software from experimental data; Ag and Cu from Palik [31], Au from Johnson and Christy [32]. The structure was simulated by using periodic boundary conditions over a unit cell under plane wave illumination. The power absorbed per unit volume is calculated by using the Poynting's Theorem for dispersive media, which for non-magnetic media simplifies as,

$$P_{abs}(\vec{r},\omega)dV = 0.5\omega\,\mathrm{Im}(\varepsilon(\vec{r},\omega))\left|\vec{E}(\vec{r},\omega)\right|^2 . \quad (1)$$

Where $E = E_i + E_s$ takes into account the incident Electric field as well as the scattered electric field by the MNP. This is integrated in the semiconductor volume, and normalized to the power injected into the simulation volume (P_{in}), yielding the normalized absorption in the PbS CQD film,

$$Abs = \int_{SC} P_{abs}dV \Big/ P_{in} . \quad (2)$$

The absorption gain in the semiconductor due to the presence of the MNPs was then defined as

$$G(\lambda) = Abs^{w.MNP} \Big/ Abs^{w/o.MNPs} . \quad (3)$$

From the spectral gain we define the average gain (η) as the average of G in a region of the spectrum where the host material absorbs (400 nm-900 nm).

#151334 - $15.00 USD Received 18 Jul 2011; accepted 13 Sep 2011; published 7 Oct 2011

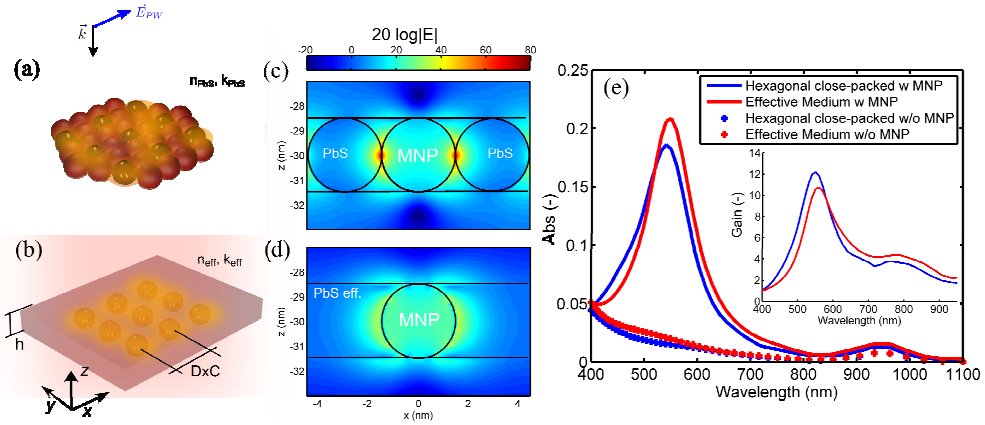

Fig. 1. Comparison between full CQD modeling and effective medium approach. (a) A monolayer section of hexagonaly.close-packed CQD (dark red) and MNPs (black). (b) The same MNP distribution inside a homogeneous effective film. The nanocomposite layers are illuminated from the top with an *x*-polarized plane wave. The concentration can be tuned by modifying the *C* factor for a given MNP size. Field intensities in a cross section of the film for (c) packed QDs and (d) effective medium. (e) Normalized absorption in the CQDs (red) and effective medium (blue) with (solid) and without (dotted) MNPs. The spectral gain is shown in the inset.

A cross section of the field intensity profile for on-resonance MNPs is shown in Fig. 1(c-d) for the HCP and effective homogenous medium models respectively. Hot spots are evident in the HCP case, highly localized to within 0.1 nm of the QD-MNP interface, but are not present with the effective medium approach. Interestingly, outside this region, in the nm scale, the shape of the field intensity is similar in both cases. In order to determine the overall effect of the differences in the near fields, the normalized absorption and gain spectra are plotted in Fig. 1(e). The absorption spectra are very similar: the peak due to the localized surface plasmon resonance (LSPR) of the particles is shifted by less than 10 nm for the effective medium case, and differences in amplitude are less than 14%. This results in a slight reduction of the average spectral gain, η, by 8% for the effective medium compared to the HCP model. These results demonstrate that although, there are differences in the near field distribution between the discrete QD and the effective medium approach, the later gives both qualitatively and quantitatively similar results and at the same time allows us to model different MNP sizes and concentrations. Moreover, experimentally, CQDs do not form perfect HCP lattices but are distributed in random close packed arrays. In these types of films, the effect of the geometry of the QD-MNP interface will be averaged out over the whole film. As such, using the effective medium approach proposed here may prove more useful in uncovering trends and probing the physical mechanisms behind near field enhancement in experimentally realizable CQD films.

2. Host medium effect

Understanding how the optical properties of the host material determine the MNPs interaction and the resulting near field absorption enhancement is of ultimate importance in optimizing this enhancement for a particular family of materials. CQDs and polymers are ideal candidates for near field enhancement studies, as their solution processability allows for straightforward integration with colloidal MNPs. Organic-based semiconductors have been considered with MNPs for plasmonically enhanced solar cells [20–23], yet CQD-based devices have remained underexplored. However, QDs and polymers have significantly different refractive indices. Polymers typically have lower *n* values around 1.6-1.8 while PbS and PbSe QDs have refractive indices of between 2 and 3. In this section we compare the efficacy of MNP-

#151334 - $15.00 USD Received 18 Jul 2011; accepted 13 Sep 2011; published 7 Oct 2011

absorption enhancement between these two classes of semiconductors and identify the most promising candidate to benefit from the exploitation of plasmonic absorption enhancement with a view to real-device geometries.

To investigate the effect of the refractive index of the host material on the optical absorption enhancement provided by embedded MNPs, we plot the gain spectra for different host materials, systematically varying the n, κ values. We model a 60 nm thick film with the geometry depicted in Fig. 1 (b), and with particle diameter D = 10 nm, and spacing C = 2. Firstly, we keep $\kappa = \kappa_{PbS,EM}(\lambda)$, and vary $n(\lambda)$, maintaining the spectral shape of $n_{PbS,EM}(\lambda)$ and normalizing it to different n values at λ = 2 μm, where $\alpha(\lambda) = 0$. Secondly, we keep $n(\lambda) = n_{PbS,EM}$, and vary $\kappa(\lambda)$ by normalizing $\kappa_{PbS,EM}(\lambda)$ to the indicated values at the exciton peak (λ = 945 nm).

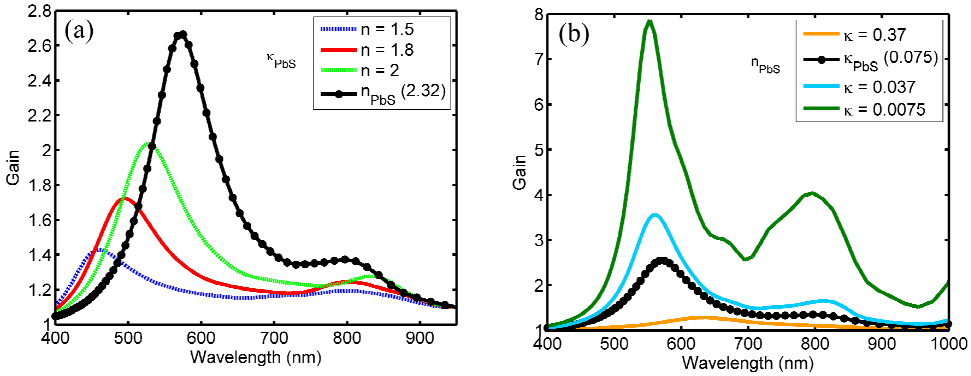

Fig. 2. Effect of the host medium optical properties on the near field enhancement, D = 10nm Ag MNPs with C = 2. (a) Modifying $n(\lambda)$, while fixing $\kappa = \kappa_{PbS,EM}$ (values in the legend correspond to $n(\lambda$ = 2μm). (b) Fixing $n = n_{PbS,EM}$ and varying $\kappa(\lambda)$, from poor to highly absorbing material, maintaining the spectral shape of $\kappa_{PbS,EM}$ but normalizing it at the exciton peak to the indicated values.

Figure 2(a) shows the calculated gain spectra for host materials with the same absorption profile as a PbS CQD film but with varying values of $n(\lambda$ = 2μm), from 1.5 (organic-like) to $n_{PbS,EM}$. Lowering the refractive index values of the host medium leads to blue shifting of the peak gain and dramatically lower absorption gains. From the quasi-static model of particle scattering [33], which is valid when $D << \lambda$, we would expect a blue-shift of the localized surface plasmon wavelength as the refractive index of the surrounding media decreases. Additionally, the magnitude of the polarisability of the MNP depends on the optical constants of both the MNPs and the host, and reduces with decreasing n. In conjunction with the blue-shifting of the plasmon resonance of the MNPs to wavelength regions where κ is larger, (hence where the potential for absorption enhancement is lower) this leads to a large reduction in the peak gain with decreasing n.

Figure 2(b) shows the gain spectra for various host materials with $n = n_{PbS,EM}$ and with varying values of $\kappa(\lambda$ = 945nm), from poor to highly absorbing material. The magnitude of the gain decreases as κ increases due to decreasing polarisability of the MNPs [25] and reduced interaction between the nanoparticles. Additionally, as mentioned above, increasing κ will reduce the potential for absorption enhancement in the material. Having materials with reduced κ will lead to higher enhancements, however if the absorption of the material is too low, losses in the MNP will dominate [9]. These results show that the gain is sensitive to both n and κ, and in evaluating the near field enhancement it is necessary to take into account the spectral dependence of the complex refractive index as well as the effect of MNPs interaction.

To analyze in detail the differences in the effect of near field enhancement in PbS-PbSe and polymer families, we compare PbS and P3HT absorption for different MNPs sizes and separations.

#151334 - $15.00 USD Received 18 Jul 2011; accepted 13 Sep 2011; published 7 Oct 2011

As above, a film thickness of 60 nm was chosen as it is experimentally feasible for CQD optoelectronic devices and allows the comparison of monolayers of various sizes of MNPs in the near field regime i.e. $D << \lambda$. The particle diameters were further limited to the size range that can be synthesized via colloidal routes [20]. The concentration of MNPs was modified though the lattice parameter, $d = DxC$, by varying C. The complex refractive index of P3HT was modeled following a similar procedure as described above for $n_{PbS,EM} + i\kappa_{PbS,EM}$, normalizing $\alpha(\lambda = 550\text{ nm})$ to 10^5 cm^{-1} from literature values [34].

Figure 3a (left) shows normalized absorption spectra for CQD PbS nanocomposite films with 10 nm diameter Ag MNP present in different concentrations defined by $1.5 \leq C \leq 4$, or equivalently area densities from 20% to 5%. The absorption in a plain PbS CQD film is given for reference. The inset graph shows the calculated gain. Reducing inter-MNP distance (thus increasing concentration), results in an increase in the normalized absorption in the wavelength region 500-700 nm, which corresponds to the LSPR of the MNPs in this medium. The increase in the gain (see inset) is accompanied by a broadening and red-shift of the peak as C is reduced, which is indicative of coupling effects among neighbouring particles [35–37]. The red-shifting of the peak is largest as C is reduced from 2 to 1.5, corresponding to particle separations of 10 and 5 nm respectively. At these separations, we are in the near-field coupling regime, where small reductions in particle separation can lead to significant changes in the resonance position absorption [37]. For all cases, absorption enhancement persists beyond the plasmon resonance of the MNPs, indicating the possibility of broadband enhancement in such nanocomposite structures. This has been observed previously by Lee and Peumans, who attributed this to non-resonant scattering by the MNPs [25].

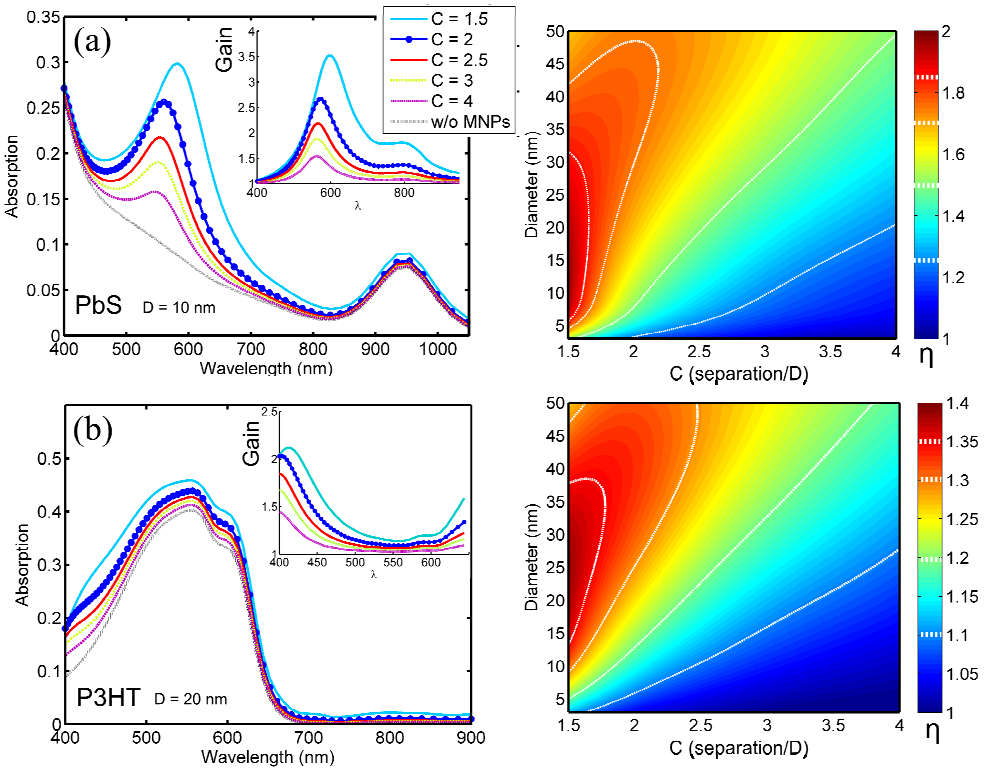

Fig. 3. Left: power absorbed in the host medium normalized to incident power for embedded Ag MNPs and different concentrations; Inset: gain derived from MNPs inclusion; Right: integrated gain (η) for Ag MNPs in the separation-size parametric space; for (a) CQD PbS host medium, and (b) P3HT host medium.

#151334 - $15.00 USD Received 18 Jul 2011; accepted 13 Sep 2011; published 7 Oct 2011

The panel on the in Fig. 3a shows the spectrally integrated absorption gain for CQD PbS films, defined in the wavelength range 400-950 nm, as a function of easily controlled parameters of MNP concentration (C) and diameter (D). Gain factors of 2 can be reached with small MNPs ($5 \leq D \leq 30$ nm), at high concentrations ($C \leq 2$). For $D < 30$ nm, the gain increases monotonically with increasing concentration and diameter, as the fraction of the host medium overlapping with the near field of the particles, and hence the absorption, increases. For larger MNP sizes (D>35nm), another regime is observed; for a given D the dependence of η on C is no longer monotonic, and the gain reduces for larger MNPs when $C < 2$. This is attributed to the fact that, while larger MNPs provide larger near field overlap with the host medium, they will also absorb more light, resulting in a reduced optimum concentration as D increases. It is clear that while larger MNPs yield lower maximum gains they allow for lower concentrations, which could be required when it comes to realizing devices experimentally.

In Fig. 3(b), a similar study was carried out for P3HT host medium. The panel on the left shows the absorption spectra for nanocomposites with 20 nm diameter Ag MNPs in different concentrations, together with the no MNP case. The inset graph shows the calculated gain. The LSPR peak of the Ag MNP is blue-shifted to λ_{res}~410 nm due to the low n_{P3HT} values and is masked due to the strong absorption in P3HT for wavelengths 400 nm<λ<650. As in Fig. 3(a), the gain increases as a function of C, but the maximum gain is reduced (G = 2.1). The average gain (η), over the wavelength range 400 to 650 nm, is shown in the panel on the right as a function of MNP size and concentration. Once again similar trends are observed as in Fig. 3(a): for D<35 nm, the gain increases as the MNP concentration and diameter are increased. However, the region of maximum η is reduced and shifted to larger particle sizes ($15 \leq D \leq 35$ nm). This is due to the high absorption coefficient of P3HT in the wavelength region of interest (400 to 650 nm); the overall gain factor is lowered as the material is already strongly absorbing, and absorption losses in the Ag are reduced [9], favoring larger particles with more near field overlap.

For a fixed host material of CQD PbS, the effect of the choice of metal for the MNPs was investigated. The absorption in the host was calculated for nanocomposite films with Au and Cu embedded MNPs. The values of maximum gain and resonance wavelengths change for different metals. The resonance wavelength of Cu and Au MNPs is similar and red-shifted compared to Ag (from 585 nm to 633 nm). Gold MNPs provide with higher maximum gain at the resonance wavelength of the MNPs (best case for D = 10 nm, C = 1.5 yielding $G^*_{Au} = 4$, $G^*_{Ag} = 3.5$, $G^*_{Cu} = 3.2$). However, both Au and Cu start introducing losses for $D \geq 20$ nm when λ<500 nm, and as the MNPs are closer this results in a reduction of the average gain for large sizes. The maximum average gain ($\eta_{Ag} = 2$, $\eta_{Au} = 1.9$, $\eta_{Cu} = 1.65$) region is contracted for these materials to $5 \leq D \leq 20$ nm. This makes Ag a more adequate material for broadband enhancement.

The comparison between CQD PbS and P3HT host materials reveals that the first family of materials is more suited for near field enhancement, also requiring smaller MNPs or smaller concentrations for the same gain. The optimization is different for each material and higher maximum gains are possible with PbS due to the favorable n,k values. More importantly, the lower and tunable bandgap of CQD PbS, together with the broadband nature of the enhancement, allows for a better exploitation of this effect. For the remainder of the paper, we will focus on CQD PbS films as the host material.

3. Gain on and off resonance

In order to further investigate the broadband nature of the absorption enhancement, we plot the field enhancement spatial profile, calculated as the ratio of the field intensity profile with and without MNPs 20 log $|E_{w\ MNPs}/E_{w/o\ MNPs}|$. In the first row of Fig. 4 (A-B-C), the absorption gain in the host is plotted together with the power absorbed in the MNPs, with D = 10 nm, for three concentrations corresponding to C = 4, 2.5 and 1.5, in columns A, B and C respectively. It is evident that MNPs are weakly absorbing beyond 700 nm, yet there is absorption

#151334 - $15.00 USD Received 18 Jul 2011; accepted 13 Sep 2011; published 7 Oct 2011

enhancement in the host medium. The gain spectra clearly show broadband enhancement extending beyond the plasmon resonance of the MNP. Similar behavior has been predicted by generalized Mie theory models, attributing this to electric field scattering in the near field by the MNPs [25].

In the second row of Fig. 4 (A1-B1-C1) we plot the spatial profile of the gain in the *x*-*z* plane of the structures at a wavelength corresponding to the plasmon resonance peak in each case, as indicated in Fig. 4 (A-C). A region of high gain surrounding the particles can be observed, accompanied by strong absorption in the Ag. The gains at the peak wavelength are given in each case showing a significant increase with decreasing inter-particle distance. It is clear that as the concentration increases the gain is more intense and localized in the x-z plane. Strong inter-particle interaction is occurring as the near fields of the MNPs increasingly overlap, leading to a localization of the gain in a narrow zone around the MNPs.

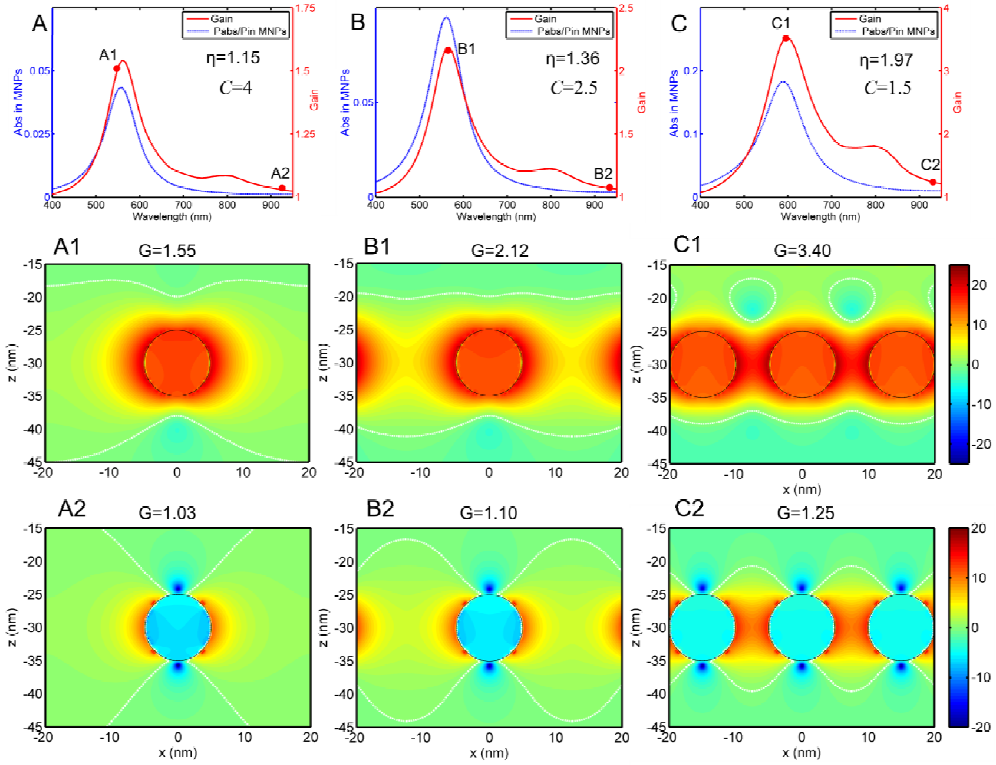

Fig. 4. Gain, power absorbed in MNPs and field enhancement spatial profile (calculated as 20 log $|E_{w\ MNPs}/E_{w/o\ MNPs}|$ [dB]) for different MNPs concentrations, for D = 10 nm Ag MNP. Columns A, B, C correspond respectively to C = 4, C = 2.5 and C = 1.5 and rows to wavelengths (on-resonance λ = 585nm row 1, off-resonance λ = 940nm row 2) as is indicated on top of each column. White dashed lines (0 dB) separate areas with positive and negative contributions to the overall absorption in PbS. The field enhancement within MNPs is representative of their losses compared to the absorption in the same volume of a homogeneous PbS film. The average gain as well as the gain at each wavelength is indicated within each panel.

In the third row of Fig. 4 (A2-B2-C2) we plot the spatial profile of the gain at a wavelength off resonance, indicated in Fig. 4 (A-B-C). At this wavelength, the MNPs are not absorbing as the skin depth of Ag is >>*D*, yet they provide gain in the host medium. Additionally, reductions in absorption are observed in plane vertical to MNP array. In the low concentration regime (A2, C = 4), the gain occurs over a large angular range in the x-z plane, which reduces as the inter-MNP distance decreases. For the highest concentration (C2, C =

#151334 - $15.00 USD Received 18 Jul 2011; accepted 13 Sep 2011; published 7 Oct 2011

1.5), most of the gain is localized in the area between the MNPs, yielding higher maximum gain factors. This finding suggests that, to maximize the gain factor achievable, an optimum thickness of the host material exists for a given particle concentration.

3. Ligand effects

In our studies so far we have assumed that the MNPs are in very close proximity to the semiconducting host medium. In reality, however, colloidal MNPs are capped with organic molecules which serve to passivate the surface of the NPs and to render them dispersible in organic solvents. These molecules typically have a thiol or a carboxyl group to attach to the MNP and a carbon atom chain whose length is ~1-2 nm. Alternatively, shorter bidentate molecules can also be employed to crosslink MNPs with QDs, with lengths on the order of 0.5 to 0.2 nm. These ligands are typically organic molecules with a refractive index of ~1.55, a value which we used in this study to optically model the ligand molecule in our structures.

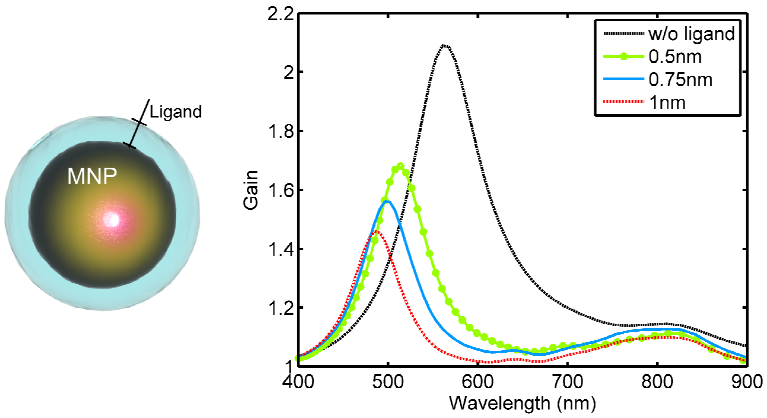

Fig. 5. Ligand effect on gain for different lengths (Δ) and Ag MNPs, fixed C = 2.5. A ligand shell with refractive index of 1.55 covers the MNP (left). Gain spectrum for D = 10 nm (right).

In Fig. 5 we plot the gain spectra in nanocomposites composed of 10 nm diameter Ag MNPs, capped with ligand shells of different thicknesses; 0.5 nm<Δ<1 nm . It is evident that a strong decrease in absorption enhancement takes place in the presence of these molecules. Additionally, a significant blue-shift of the plasmon peak of the MNP is observed with increasing ligand length as a result of the lower refractive index of the ligand molecule, which affects the effective refractive index of the host medium in the vicinity of the MNP. For a ligand with Δ = 0.5 nm, the maximum on resonance gain (shifted from 565nm to 513nm) is reduced by 20%, however only a 2.5% reduction is observed at wavelengths off-resonance (around 800nm). To investigate the origin of this reduction we study the modification of the near fields when the ligands are introduced.

Figure 6 shows the field enhancement spatial profile as well as the decay of field intensity $|E|^2$ from MNPs surface at wavelengths both on (565 nm and 490 nm) and off (820 nm) resonance. For a bare MNP at a wavelength on resonance [Fig. 6(a)], the field enhancement is maximum at the metal/semiconductor interface and decays with the distance away from the MNP. However, when a ligand is introduced [Fig. 6(b)] the maximum field is highly confined in the ligand volume, and does not contribute to the absorption in the semiconductor. From the Fig. 6(c), it is clear that the introduction of the ligands reduces the maximum field enhancement in the host by approximately by 10 dB. While the dependence of the field intensity with distance is similar for all ligands lengths, a larger fraction of field is confined in larger ligand volumes. We attribute this confinement and enhancement of light in the ligands, to large discontinuities in the electric fields at high index-contrast interfaces [38]. This strong

#151334 - $15.00 USD Received 18 Jul 2011; accepted 13 Sep 2011; published 7 Oct 2011

confinement behavior has been seen previously, albeit in other geometries, with large field enhancements calculated in thin dielectric layers, in the vicinity of a MNP [16].

From Fig. 6(d-f) it is evident that confinement of the enhanced optical fields in the ligand is occurring at wavelengths off resonance as well, with a similar dependence on ligand length. However, suppression of the fields that occur perpendicular to the plane of the MNP array, and that contribute negatively to gain in Fig. 6(d), are also confined within the ligand shell in Fig. 6(e), reducing the detrimental effect of ligand introduction off resonance.

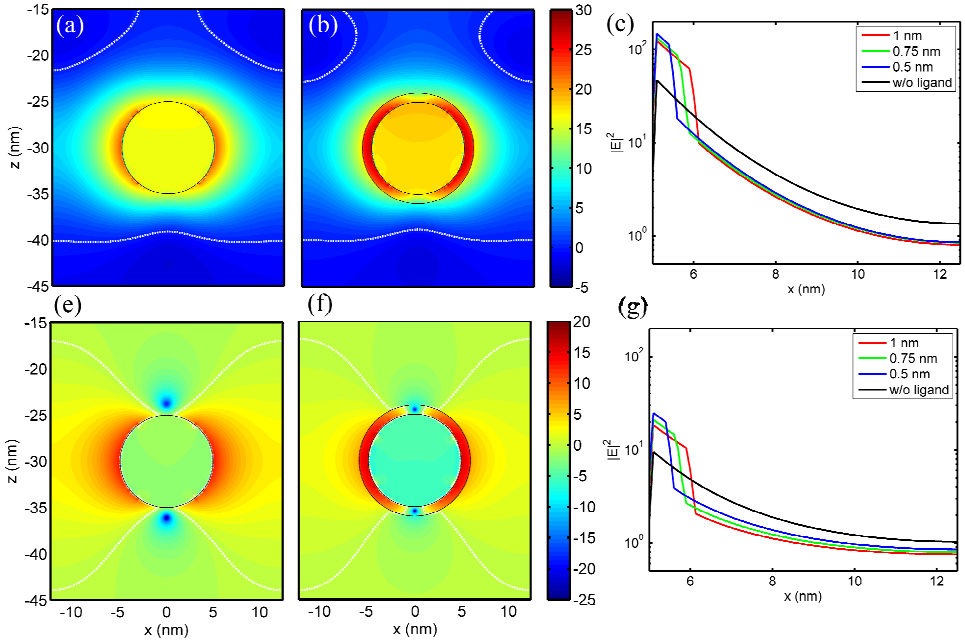

Fig. 6. Field enhancement spatial profile, for D = 10 nm Ag MNP and C = 2.5. (dB scale). (a) no ligands on resonance, (b) Δ = 1nm on resonance, (c) $|E|^2$ decay from MNP surface on resonance no ligands on resonance, (d) no ligands off resonance (e) Δ = 1nm off resonance, (f) $|E|^2$ decay from MNP surface on resonance.

We conclude that the observed 20% on resonance reduction in gain due to the inclusion of a ligand has a threefold origin. Firstly the ligand introduces a spacer layer around the particle, reducing the overlap of the increased optical near field with the absorbing host medium. Secondly, the field is effectively confined in the low refractive index ligand, close to the nanoparticle surface, which reduces the maximum field enhancement, and hence the gain, in the host. Thirdly, the inclusion of the lower refractive index ligand shifts the plasmon resonance of the MNP to shorter wavelengths, where CQD PbS has higher κ values and there is less potential for absorption enhancement. At wavelengths off-resonance, the introduction of a ligand results is a lower reduction in gain of only 2.5%. This is due to the fact that the gain is less sensitive to the position of the resonance wavelength, and areas of field suppression as well as gain are confined within the ligand

While the reduction of gain due to the ligand acting as a space layer is hard to overcome, we hypothesized that we can vary the refractive index of the ligand to recover some of the losses in gain. We thus studied the effect of the refractive index of the ligand considering alternative capping schemes based on inorganic layers that can be employed to overcoat the MNPs such as silica and titania [23].

In Fig. 7 (a) we plot absorption gain spectra for various values of the refractive index of the ligand. As expected, we observe a significant increase of the on resonance gain for increasing ligand refractive index. From the field enhancement profiles, plotted in Fig. 7 (b)

#151334 - $15.00 USD Received 18 Jul 2011; accepted 13 Sep 2011; published 7 Oct 2011

for n_{lig} = 1.5 and (c) for n_{lig} = 2.5, it is clear that the enhanced optical fields are less localized in the ligands for n_{lig} = 2.5, resulting in the recovery of the gain. This is consistent with the physical origin of the confinement of the near field in the ligand introduced above; as the refractive index of the ligand is increased, the index contrast is reduced, and the field is less confined to the ligand. Additionally, from Fig. 7 (a), the LSPR of the capped MNP is red-shifted as n_{lig} is increased: for the case of n_{lig} = 3, which is larger than $n_{PbS,EM}$, the resonance peak is further red-shifted with respect to the bare MNP case, to wavelengths at which $\kappa_{PbS,EM}$ is lower and the absorption enhancement potential is higher.

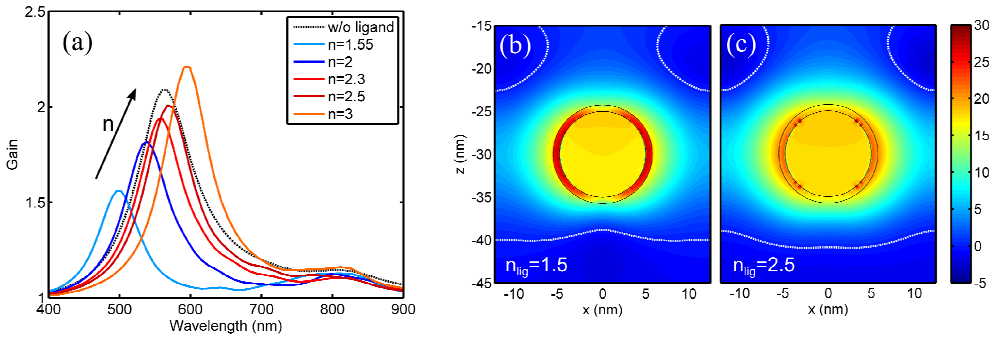

Fig. 7. Effect of ligand refractive index for D = 10nm Ag MNPs C = 2.and Δ = 0.75 nm (a) Gain comparison from organic to inorganic coatings. Field enhancement spatial profile (in dB) for D = 10 nm Ag MNPs and Δ = 0.75 nm ligand of refractive index (b) 1.5 (organic) and (c) 2.5 (titania).

From these results, it is clear that both field confinement and the blue-shifting of the resonance wavelength due to the presence of the ligands are important loss mechanisms for on resonance gain. For wavelengths off-resonance, the gain is less sensitive to the resonance wavelength and to the field confinement, as areas of field enhancement and suppression are confined in the ligands. As we have demonstrated, a careful choice of the ligand plays a central role in maximizing absorption enhancement in metal-semiconductor nanocomposites.

5. Conclusions

In summary, we have presented a full wave 3D simulation study of absorption enhancement in solution processable semiconductor – MNP nanocomposite structures. We introduced an effective medium model to simulate the optical constants of CQDs films. This approximation enables the simulation of a variety of MNP sizes and concentrations in nanocomposite films, permitting the investigation of the underlying trends in near field enhancement. Employing this effective medium approach we demonstrate the importance of the optical properties of the host medium in determining the near field enhancement and confirm that CQD PbS films are ideal candidates for near field enhancing. Absorption enhancements of over 100%, compared to quantum dot only structures can be achieved in the visible-near infrared region by careful design and selection of material parameters, paving the way for more efficient quantum dot solar cells. We identify the origin of the detrimental effects of MNP capping as due to the overlap and confinement of the enhanced optical fields in the low refractive index ligands and the shifting of the surface plasmon resonance wavelength. We demonstrate that on resonance gain can be recovered by careful choice of ligand refractive index. Our study is limited in the optical domain, neglecting exciton quenching effects and energy back-transfer from QDs to MNPs. However these preliminary results point to further investigation of these structures for the demonstration of plasmonically enhanced all-solution processed optoelectronic devices.

Acknowledgements

This research has been partially supported by Fundació Privada Cellex Barcelona.

#151334 - $15.00 USD Received 18 Jul 2011; accepted 13 Sep 2011; published 7 Oct 2011